Microstructural evolution during direct laser sintering in the Al_2O_3–SiO_2 system

**Jürgen G. Heinrich · André Gahler · Jens Günster ·
Martin Schmücker · Jingxian Zhang · Dongliang Jiang ·
Meiling Ruan**

Abstract The microstructural evolution during direct laser sintering of LSD (Layerwise Slurry Deposition)—samples in the Al_2O_3–SiO_2 system has been investigated. Slurries with a water content of 34 wt.% and a SiO_2/Al_2O_3—ratio of about 3:1 have been used to manufacture layers which—after consecutive drying—have been sintered and laminated by laser treatment. Densified samples can be obtained with laser irradiances from 190 to 270 kW/cm^2 and scan velocities between 35 and 65 mm/s. Elemental mappings of the layers' cross sections suggest an inhomogeneous phase distribution in the laser sintered LSD samples with a slight alumina concentration gradient. A lower degree of particle melting in the bottom region of the layers is plausible due to attenuation of the laser beam intensity. SEM and HRTEM micrographs show that after a few seconds of laser treatment relictic starting phase, crystalline alumina plus amorphous silica, occur together with needle like mullite, the latter formed within an amorphous aluminosilicate phase. The resulting phase assemblage reflects the non-equilibrium conditions which can be expected for short time laser treatments. Mullite nucleation within the bulk of the liquid phase rather than in the vicinity of the parent alumina phase suggests that dissolution of alumina is the rate controlling step. Subsequent thermal post treatment in air in a conventional sintering furnace causes an increase of density to about 96% and leads to additional phase reactions. Amorphous silica transforms into cristobalite and the amount of alumina is reduced by additional mullite formation. By both coalescence of individual crystals and grain growth the morphology of the newly formed mullite changes during post heat treatment.

J. G. Heinrich · A. Gahler (✉)
Institute of Non-Metallic Materials,
Clausthal University of Technology, Clausthal-Zellerfeld,
Germany
e-mail: andre.gahler@tu-clausthal.de

J. Günster
Laser Application Centre, Clausthal University of Technology,
Clausthal-Zellerfeld, Germany

M. Schmücker
German Aerospace Center, Cologne, Germany

J. Zhang · D. Jiang · M. Ruan
Shanghai Institute of Ceramics, Chinese Academy of Sciences,
Shanghai, P.R. China

Introduction

In the last two decades several processes of solid freeform fabrication have been developed for manufacturing ceramic prototypes using lasers as energy sources [1–6]. Customer demands should be met with these technologies by shortening the period of time between design of ceramic components and testing. The most attractive methods among those are direct laser sintering processes which lead to near net shape components from a computer file without the need of models and molds.

The first techniques developed typically either provided green bodies with high contents of organic, inorganic or metallic binders [2, 6] or resulted in components with high amounts of porosity where no binders were used [7, 8]. In both cases fluffy structures resulting from a powder bed with a low green density were responsible for low sintered densities. To increase the density of both green and the sintered bodies the LSD (Layerwise Slurry Deposition) and the LSS (Laser Surface Sintering) techniques have been

developed with conventional molding technologies being adapted to the laser sintering process [9, 10]. In systems with liquid phases being present during laser sintering almost theoretical dense products can be achieved with these methods. The liquids formed during sintering enhance the wetting of the different layers leading to improved lamination [11, 12].

However, it is not well understood up to now whether or not the densification mechanisms during laser sintering with a very short sintering time are comparable to those during conventional sintering. It is also unclear how fast phases are formed during laser sintering and if it is possible to tailor microstructures because of the extremely short sintering times.

This paper presents first studies on the microstructural evolution during direct laser sintering of LSD—samples in the Al_2O_3–SiO_2 system. The appearance of a liquid phase above 1,600 °C makes materials in the SiO_2 rich region of the phase diagram most suitable for getting dense components by direct laser sintering. Liquid phase sintering mechanisms can be expected like the mullite formation via a dissolution-precipitation process. After some laser parameter studies the microstructural development will be discussed on the example of X-ray, SEM, EDX, and HRTEM investigations.

Experimental

Suspensions for the layerwise slurry deposition were produced from 68.5 wt.% pure amorphous silica with a d_{50} of 11.1 μm (Mitsubishi, Japan), 25.5 wt.% pure α-alumina with a d_{50} of 1.7 μm (Nabaltec GmbH, Schwandorf, Germany) and 6.0 wt.% highly dispersed silica with aggregates of about 0.2 nm (Wacker-Chemie GmbH, Burghausen, Germany). The shape of the alumina powder is spherical whereas the silica is non-spherical. The deionized water content of the slurry amounts to 34 wt.%. The highly dispersed silica acts as a spherical stabilizer and prevents agglomeration of suspended silica and alumina particles. The electrokinetic and rheological characterization of the slip has been presented elsewhere [13].

Similar to a tape casting process, the slurry is deposited via a doctor blade on a preheated ceramic tile. The doctor blade is controlled by a robot, that facilitates a wide range of the deposition parameters. Layers with a thickness of about 100 μm have been successfully assembled to multilayer components by laser sintering. A detailed description of the LSD process can be found in ref. [14].

A laser system combining a Rofin Sinar SC 10 CO_2 laser tube (100 W) and a galvano-scanner (hurrySCAN, Scanlab AG, Germany) has been used for the experiments. The beam diameter was approximately 100 μm in the focal point. The laser system has a continuous wave nature in order to generate a high heat transfer. Although the temperature could not be measured in the focal point vaporization or decomposition could be avoided by controlling the irradiance in the focal point. The irradiance is defined as the quotient between laser power and the cross section area of the laser beam. In order to control the homogeneous layerwise build up of samples the irradiance, the laser scan lines overlapping and the scan velocity have been optimized. Almost dense samples could be achieved at irradiances between 180 and 270 kW/cm^2. A detailed description of the laser parameter studies can be found in ref. [13].

The microstructural characterization has been carried out by X-ray (Siemens Diffraktometer D5000, Siemens AG, Karlsruhe, Germany), SEM (CamScan CS4, Cambridge, UK) and EDX (Tracor Northern Typ 5402, Middleton, Wisconsin, USA) investigations. Thin foils (3 mm in diameter) for TEM were prepared by cutting and polishing (till 20 μm in thickness) and followed by argon-ion-milling until perforation. The morphology and size of the precipitates were examined using transmission electron microscopy (JEM-2100F, JEOL, Tokyo, Japan). High-resolution transmission electron microscopy (HRTEM) images and electron diffraction data were also obtained on this instrument. The accelerating voltage of the electron beam was 200 keV.

Results and discussion

In the silica rich area of the SiO_2–Al_2O_3 phase diagram studied in this investigation liquid phase formation can be expected above 1,600 °C. Liquid phases promote the sintering velocity and are therefore predestinated for short sintering times as they occur during laser sintering. The layerwise slurry deposition followed by direct laser sintering leads to densified microstructures in this system in the parameter field shown in Fig. 1. Even if the sintering temperature could not be measured it can be understood that low values of irradiance, scan velocity and laser track overlapping lead to unstable parts because of too low sintering depth followed by delamination. High values of irradiance are limited by vaporization or decomposition of the material to be sintered. In order to avoid vaporization at high irradiances, the scan velocity can be increased and/or scan spacing can be reduced. Densified samples could be achieved at irradiances from 180 kW/cm^2 to 270 kW/cm^2 and scan velocities between and 65 mm/s. After laser sintering the density of the ceramic samples varies between 86 and 92% th.d. The open porosity of the samples has been determined to be between 10 and 14%. The maximum pore diameter amounts to about 30 μm. The SEM
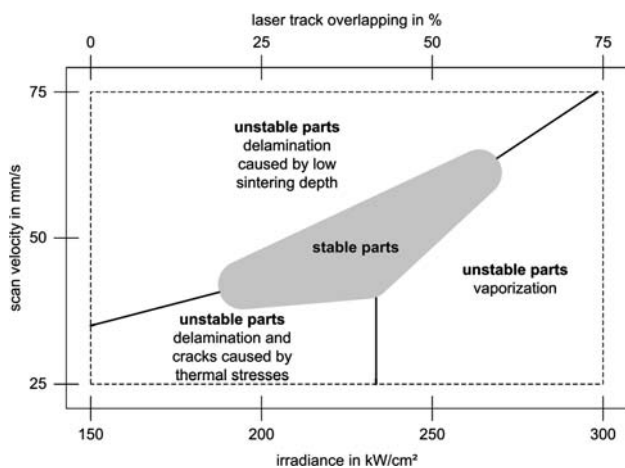
Fig. 1 Illustration of the optimal parameter field for laser sintering of Al$_2$O$_3$–SiO$_2$ powder mixtures

micrographs of the layers' cross sections suggest an inhomogeneous phase distribution in the laser sintered LSD samples (Fig. 2). EDX spectra suggest that in the upper
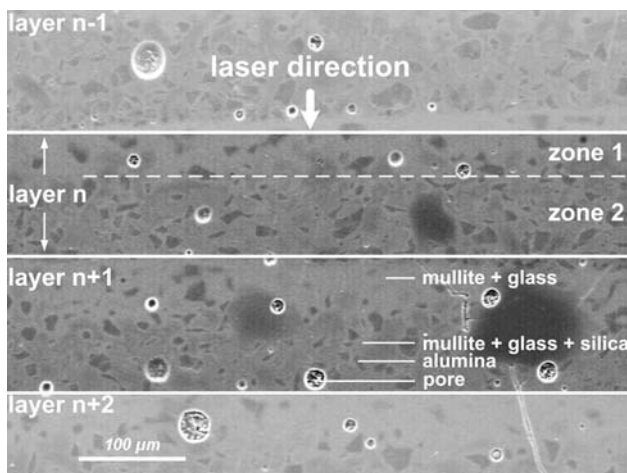
Fig. 2 Typical cross section of a LSD sample treated with 250 kW/cm^2 showing an inhomogeneous phase distribution (polished, etched, SEM, SE)
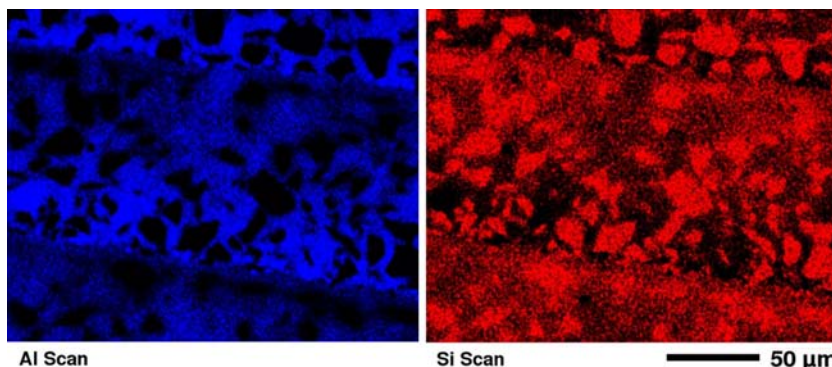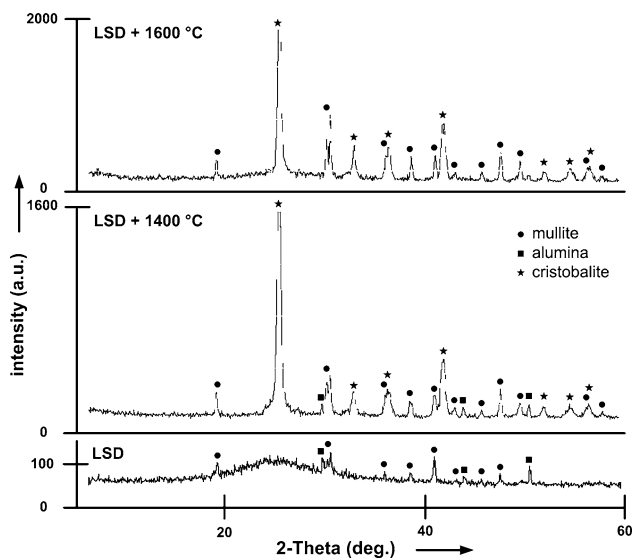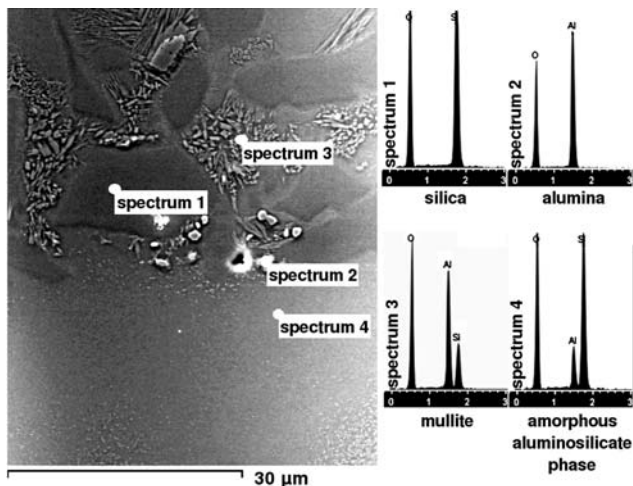
part of the laser sintered layers where the laser first meets the layers during sintering mullite and a glassy phase appear. In the lower parts unreacted alumina arises together with relicted silica, mullite and glass.

Elemental mappings of these layers confirm the inhomogeneities with a slight alumina concentration gradient (Fig. 3). Obviously, the average alumina concentration decreases in going from the bottom of an individual layer to its top. The resulting phase assemblage reflects the non-equilibrium conditions which can be expected for short time laser treatments. In general, the amount of unmelted starting particles is higher in the layer's bottom zone than in the top zone. This comes especially true for relictic alumina particles, which are only found in the bottom regions of individual layers. The lower degree of particle melting in the bottom region is plausible due to strong attenuation of the laser beam intensity near the surface and the ineffectual heat transfer in ceramic materials. The observed compositional demixing can be understood in terms of segregation caused by higher specific weight of corundum.

XRD of the LSD samples proves two crystalline phases, mullite and alumina (Fig. 4). A glassy phase can also be estimated by the peak elevation at about 25 degrees 2 theta. Scanning electron micrographs together with EDX analysis show besides alumina and mullite relicted amorphous silica and a newly formed amorphous aluminosilicate phase. SEM investigations reveal that mullite formation occurs virtually homogeneous inside the aluminosilicate melt that spreads between not fully dissolved alumina and silica grains (Fig. 5). Newly formed mullite often displays needle-type crystals. This is the typical appearance of mullite formed from silica-rich starting compositions [15]. The elongated direction corresponds to the crystallographic c-axis of mullite (e.g. [16, 17]). Previous studies on reaction sintering of mullite showed that mullite formation occurs via a dissolution-precipitation process. Heating alumina–silica powder mixtures leads to the formation of a siliceous melt which

Fig. 3 Elemental mappings of the layers' cross sections demonstrating the inhomogeneous phase distribution in LSD samples (SEM/EDX)

Fig. 4 X-ray diffraction phase analysis of laser sintered and post heat-treated LSD-samples

Fig. 5 SEM/EDX results showing relictic starting phases silica (spectrum 1) and alumina (spectrum 2) together with mullite (spectrum 3), the latter formed within an (amorphous) aluminosilicate phase (spectrum 4)

Fig. 6 Left: TEM micrograph showing elongated mullite needles inside an amorphous aluminosilicate phase. Right: HRTEM images of mullite needles surrounded by an amorphous aluminosilicate phase
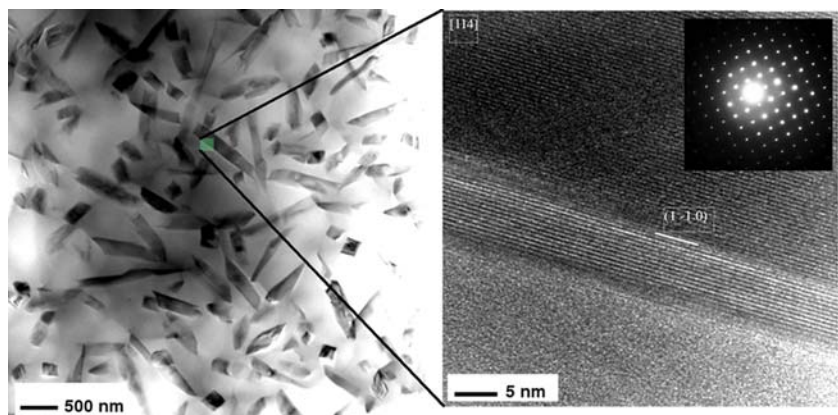
incorporates Al_2O_3 by subsequent dissolution of the starting alumina. As soon as a critical Al_2O_3 concentration is reached, mullite nucleates within the bulk of the melt [18]. Mullite formation within a liquid phase rather than by epitactic nucleation on the surface of the crystalline parent phase has been explained in terms of short-range similarities between mullite and non-crystalline aluminosilicate with dissolution of alumina being the rate controlling step. These ideas are in accordance to the microstructural characteristics shown in Fig. 6. Closer inspections by TEM supports the SEM findings and shows clearly that the mullite nucleation occurs within the liquid phase. Almost all elongated mullite grains are surrounded by an amorphous aluminosilicate phase (Fig. 6a). Typically mullite needles show elongated grains with a width of 100–200 nm and an aspect ratio of about 2.5–3. HRTEM and electron diffraction analysis indicates the crystalline mullite phase together with the amorphous surrounding (Fig. 6b). The d-values of the crystalline phase correspond well-defined with mullite, JCPDS-cart No. 15-0776.

Subsequent thermal post treatment in air in a conventional sintering furnace causes an increase of density to about 96% and leads to additional phase reactions. At 1,400 °C/2 h amorphous silica transforms into cristobalite and the amount of alumina is reduced by additional mullite formation. After a post treatment at 1,600 °C/2 h alumina totally disappears (Fig. 4). The morphology of mullite changes at 1,600 °C by coalescence of individual crystals and grain growth during post heat treatment. Equiaxed crystal sections (Fig 7a), i.e. mullite needles with x-plane orientation show the typical lattice figures of the mullite a/b plane (Fig. 7b). An amorphous aluminosilicate phase is still existing in the surrounding of the mullite crystals. All investigations surprisingly indicate that virtually within a few seconds during laser sintering dissolution-precipitation seems to be the formation mechanism of mullite as it can be observed during conventional sintering as well.

Fig. 7 Left: TEM results of a thermal post treated LSD sample showing mullite needles formed during laser sintering as well as mullite agglomerates formed during post heat treatment (250 kW/cm^2, 1,400 °C in air, TEM). Right: HRTEM images of mullite agglomerates surrounded by an amorphous aluminosilicate phase
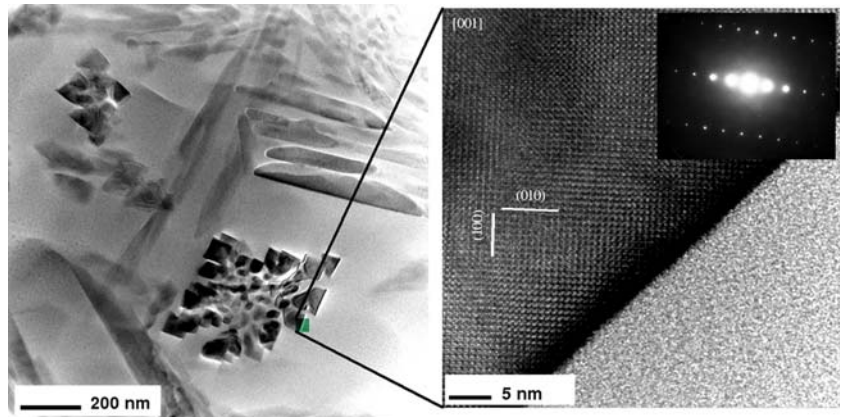
Conclusion

During direct laser sintering of LSD—samples in the Al$_2$O$_3$–SiO$_2$ system a siliceous melt is formed within a few seconds, which incorporates Al$_2$O$_3$ by subsequent dissolution of the starting alumina. As soon as a critical Al$_2$O$_3$ concentration is reached, mullite nucleates within the bulk of the melt. The dissolution-precipitation process typical for reaction sintering of mullite and subsequent unhindered grain growth leads to mullite needles. Coalescence of individual crystals and further grain growth leads to changes in the morphology during post heat treatment. The surprising fast microstructural evolution leads to the idea of tailoring microstructures by laser sintering to optimize the properties of ceramic materials. This will be a topic of further investigations.

References

1. Halloran JW, Griffith M, Chu T (2000) US patent application 6,117,612
2. Bertsch A, Jiguet S, Renaud P (2004) J Micromech Microeng 14:197
3. Stierlen P (1999) German patent application DE 198 09 657 A1, in German
4. Subramanian PK (1995) Selective laser sintering of alumina. Ph.D. Thesis, The University of Texas at Austin
5. Knitter R, Bauer W, Göhring D (2003) J Mech Eng Sci 217:41
6. Lee I. (1998) J Mater Sci Lett 17:1907
7. Löschau W, Lenk R, Scharek S, Teichgräber M, Nowotny S, Richter C (1999) In: Proc. 9th Cimtec World Ceramic Congress, p 567
8. Noeken S, Wagner C (2002) Maschinenmarkt 105:34, in German
9. Günster J, Engler S, Heinrich JG (2003) Eur Ceram Soc Bull 1:25
10. Gahler A, Günster J, Heinrich JG (2006) In: Proc. 1st Int. Congress on Ceramics, Toronto
11. Lawrence J, Li L (1999) J Phys D: Appl Phys 32:1075
12. Das S (2003) Adv Eng Mater 5(10):701
13. Gahler A, Günster J, Heinrich JG J Am Ceram Soc submitted for publication
14. Günster J, Engler S, Heinrich JG (2003) Bull Eur Ceram Soc 1:25
15. Komarneni S, Schneider H, Okada K (2005) In: Schneider H, Komarneni S (eds) Mullite, Wiley, VCH, p 251
16. Meng J, Cai S, Yang Z, Yuan Q, Chen Y (1998) J Eur Ceram Soc 18:1107
17. Deer W, Howie RA, Zussman J (eds) (1997) Rock-forming minerals, vol. IA, 2nd edn. Geological Society Publishing House, Bath, UK
18. Schmücker M (2005) In: Schneider H, Komarneni S (eds) Mullite, Wiley VCH, p 93